LETTERS

Mega-impact formation of the Mars hemispheric dichotomy

Margarita M. Marinova[1], Oded Aharonson[1] & Erik Asphaug[2]

The Mars hemispheric dichotomy is expressed as a dramatic difference in elevation, crustal thickness and crater density between the southern highlands and northern lowlands (which cover ~42% of the surface)[1,2]. Despite the prominence of the dichotomy, its origin has remained enigmatic and models for its formation largely untested[3–5]. Endogenic degree-1 convection models with north–south asymmetry are incomplete in that they are restricted to simulating only mantle dynamics and they neglect crustal evolution, whereas exogenic multiple impact events are statistically unlikely to concentrate in one hemisphere[6]. A single mega-impact of the requisite size has not previously been modelled. However, it has been hypothesized that such an event could obliterate the evidence of its occurrence by completely covering the surface with melt[7] or catastrophically disrupting the planet[3,8]. Here we present a set of single-impact initial conditions by which a large impactor can produce features consistent with the observed dichotomy's crustal structure and persistence. Using three-dimensional hydrodynamic simulations, large variations are predicted in post-impact states depending on impact energy, velocity and, importantly, impact angle, with trends more pronounced or unseen in commonly studied smaller impacts[9]. For impact energies of ~(3–6) × 10^{29} J, at low impact velocities (6–10 km s^{-1}) and oblique impact angles (30–60°), the resulting crustal removal boundary is similar in size and ellipticity to the observed characteristics of the lowlands basin. Under these conditions, the melt distribution is largely contained within the area of impact and thus does not erase the evidence of the impact's occurrence. The antiquity of the dichotomy[10] is consistent with the contemporaneous presence of impactors of diameter 1,600–2,700 km in Mars-crossing orbits[3], and the impact angle is consistent with the expected distribution[11].

The martian dichotomy may be defined by topographical, morphological and structural characteristics. Isostatic modelling combining gravity and topography have provided a description of global crustal thickness in which the northern lowlands are distinguished from the southern highlands by a reduction in crustal thickness of ~30 km (ref. 1). By accounting for lithospheric stresses, it is possible to compute the effects of overlying loads, in particular of the largest load represented by the Tharsis province. When the loads are separated, the lowlands are remarkably well described by an ellipse with dimensions ~10,650 km × ~8,520 km (ellipticity ~1.25) (ref. 2). The boundary is expressed as steep scarps in some longitudes and as gentle slopes in others[3,12,13]; significant crustal thickening is not observed at the boundary. Geochemical evidence and surface-crater densities show that the dichotomy formed within the first 50 Myr of Solar System formation, with little mantle-crust remixing since[1,10,14]. Subsequent events, such as known impact-basin formation, have modified the dichotomy boundary.

The mega-impact formation hypothesis is supported by geologic evidence including massifs and narrow plateaux concentric to the dichotomy boundary[3], steep scarps at the boundary, and by the similarity of the lowlands to other large impact basins such as South Pole–Aitken basin on the Moon, Caloris basin on Mercury and Hellas basin on Mars. The impact hypothesis has previously been challenged by several arguments. First, by the expectation that at the relevant energy, the impact would disrupt the planet sufficiently to effectively erase evidence of the event[3]. Second, by the circularity of craters for all but the most oblique angles for smaller impacts[15]. Third, by the lack of crustal thickening in an annulus around the basin, typical for smaller impacts. However, craters resulting from planetary-scale impacts have until now not been accurately modelled. This class of impacts is distinguished from the more thoroughly studied smaller impacts, which effectively form in a half-space target, in part because of the importance of surface curvature in the larger size regime and the larger fractional size of the projectile relative to the target.

Single, planetary-scale impact events are simulated using a three-dimensional self-gravitating smoothed particle hydrodynamics (SPH) code[16–18]. Our simulations sample a large parameter space, with impact energies of (0.1–5.9) × 10^{29} J, which is representative of, according to traditional scaling laws[3,9], nominal impact crater diameters of 4,000–12,000 km. For comparison, the energy of the Moon-forming impact[18] was ~10^{31} J. For each impact energy, we consider impact velocities of 6–50 km s^{-1}, ranging from near escape velocity to twice Mars's orbital velocity, and impact angles of 0 (head-on), 15, 30, 45, 60 and 75° for each velocity (Supplementary Information). For this parameter space, impactor diameters range from 400 to 2,700 km. Figure 1 schematically shows a summary of the results and the 'sweet spot' simulations that produce a crustal excavation feature remarkably similar to the lowlands.

The pre-impact resolution (particle size or smoothing length) is 118 km for $N = 200{,}000$ particles. The model uses the semi-empirical Tillotson equation of state[19] (EOS). We derived EOS parameters to approximate the behaviour of olivine, to match the planet's pressure–density profile. The olivine EOS results in a realistic early Mars internal energy–pressure profile, allowing calculation of post-impact melt using the pressure-dependent forsterite liquidus curve as an internal energy melting threshold[20]. The pre-impact planet has no initial spin: Mars's current rotational period is long compared with the timescale of the impact process. The crust is defined as the planet's pre-impact outermost particle layer, resulting in a crustal thickness of ~140 km, compared with recent estimates of 5–90 km (ref. 1). Because of the large particle size, the simulations cannot directly resolve the crustal thickness. However, the region of complete crustal removal may be mapped and the boundary of the crustal anomaly is expressed over a lateral distance of only several resolution elements.

[1]California Institute of Technology, Division of Geological and Planetary Sciences, MC 150-21, Pasadena, California 91125, USA. [2]Earth Sciences Department, University of California, Santa Cruz, 1156 High Street, Santa Cruz, California 95064, USA.

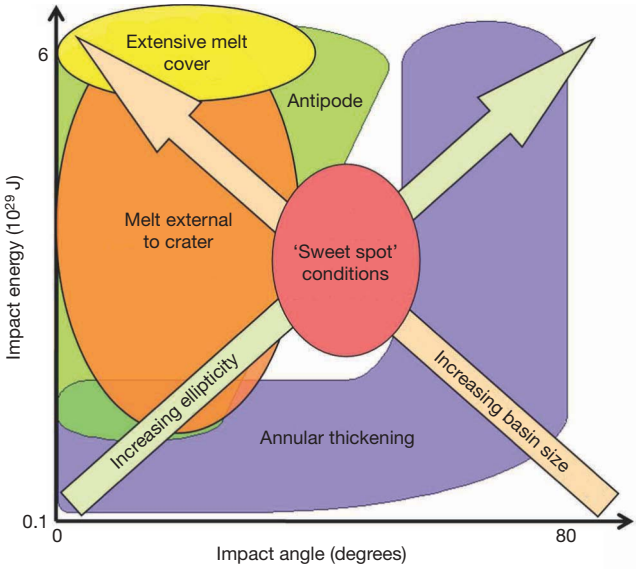

Figure 1 | Summary of simulation results. Shown are the impact characteristics resulting in extensive surface melt cover (>25% of the surface), significant melt outside the crustal excavation boundary, presence of antipodal crustal disruption, presence of a thickened annulus of crust around the crustal excavation boundary, and the directions of increase in ellipticity and basin size. The results at a given energy are averaged over impact velocity. A 'sweet spot' of impact conditions emerges for which the resulting simulation characteristics closely match the observed Mars dichotomy features[2]. A compatible hypothesis is found at an impact energy of $\sim 3 \times 10^{29}$ J, velocity ~ 6 km s^{-1} and, importantly, an impact angle of $\sim 45^{\circ}$. These parameters represent probable impact conditions in the early Solar System[3,11].

Thus the computed crustal excavation boundary size is a robust result. In addition to this boundary, we consider the integrated amount and spatial distribution of melt, crustal thickening and the extent of antipodal disruption.

The distribution of crust and surface melt are calculated as a fraction of the material within the top 150 km. An ellipse is fitted to the crustal excavation boundary (the contour of 50% crustal fraction) in polar coordinates, with the origin centred on the excavated region. Our analysis of the impact melt and its distribution shows that previous assumptions about melting during planetary-scale cratering events have been oversimplified.

In contrast to smaller, half-space craters, whose size and melt production dominantly scale with the impact energy[21], for planetary-scale impacts we find that impact velocity and impact angle fundamentally affect the crustal excavation boundary, its ellipticity, and the amount and distribution of melt. In particular, we identify possible impacts that are consistent with the crustal distribution of Mars.

Planetary-scale impacts penetrate into the mantle. The resulting rarefaction wave completely removes the surrounding crust, which re-impacts elsewhere on the planet or is ejected to space. The size of the crustal excavation boundary is representative of the size of the crustal thickness dichotomy that is likely to remain, neglecting later geologic crater modification. Simulation results show that the crustal excavation boundary size increases with increasing impact energy. For a given impact energy, the boundary size decreases with increasing velocity and with increasingly oblique impacts (Figs 2 and 3a). For smaller, half-space impact craters, a deviation in circularity is only present for highly oblique impacts[9,15] (>80°). In contrast, our planetary-scale impact simulations show that with increasing impact energy, the removed crustal region becomes significantly elongated at relatively shallow angles (Fig. 3b).

The pattern of crustal redistribution depends upon impact angle. Although angles above ~60° result in a distinct rim-like feature, less oblique impacts (<45°) produce widespread crustal thickening but no short length-scale variations, in agreement with dichotomy characteristics (Fig. 4; contrast with Supplementary Information). In cases with high ejection velocity, the flight path of ejected material is of the order of the radius of the planet; thus the ejected material is distributed globally.

Melt production and distribution are also strongly dependent on impact energy, velocity and angle. The total amount of melt increases with increasing impact energy, and at constant energy and low impact angles exhibits a weak maximum at intermediate velocities (10–20 km s^{-1}). Melt significantly decreases with increasing impact angle. As an example, for a nominal 10,000-km crater, head-on (0°) impacts produce a Mars global equivalent layer (GEL) melt depth

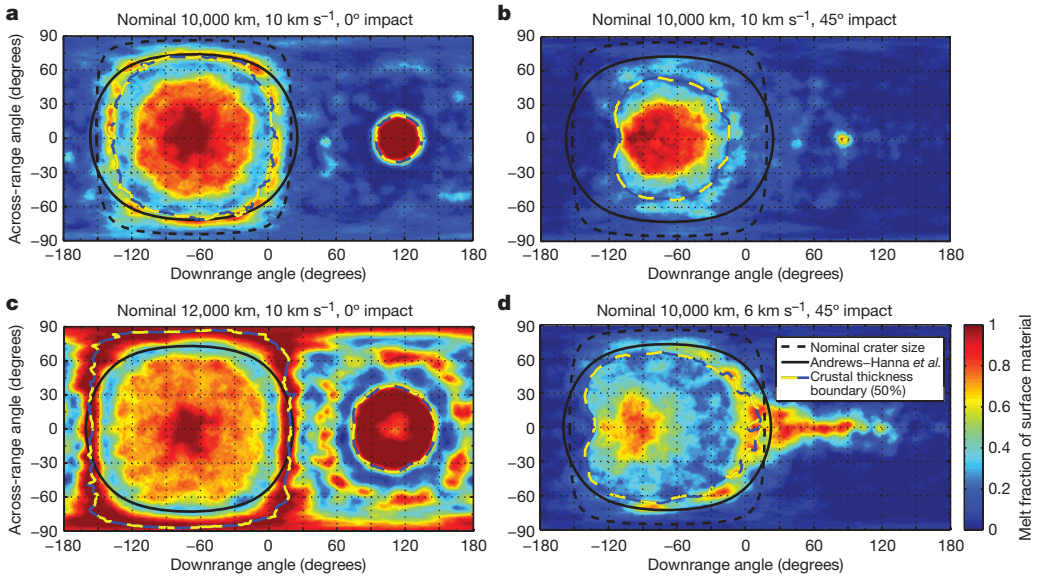

Figure 2 | Change in melt distribution and crustal removal boundary with impact characteristics. Crustal excavation boundary, nominal crater size and a fit by Andrews-Hanna *et al.*[2] to the dichotomy boundary are overlaid. The melt distribution is computed at a 2° resolution and smoothed over a 10° diameter cap area. The surface melt cover fractions are 25%, 8%, 71% and 12%, respectively. Note the changes in features with impact energy (nominal crater size), velocity and angle. The planet has been rotated to centre the excavation boundary at approximately −60° downrange angle.

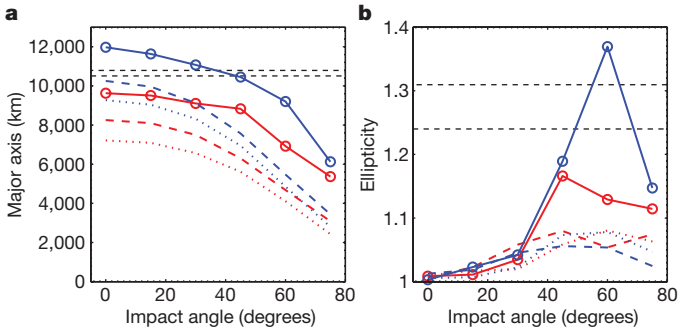

Figure 3 | Major axis and ellipticity for impact energies of 3. 1×10^{29} J and 5.9×10^{29} J (red and blue, respectively). a, Excavated cavity major axis; **b**, ellipticity. Shown are impact velocities of 6 km s^{-1} (solid line), 10 km s^{-1} (dashed line) and 50 km s^{-1} (dotted line). Major axes and ellipticities of mapped dichotomy boundary ellipse fits[2] are shown (black dashed lines), representing the range of possible boundary locations (reported uncertainty of ± 100 km). A 'sweet spot' emerges for these impact energies and at impact velocities of 6–10 km s^{-1} and impact angles of 30–60°.

of 60–80 km (depending on impact velocity), whereas 75° impacts produce a GEL melt depth of only 6–20 km. The vaporized mass is less than 1% of the molten mass.

Global melt depths of tens of kilometres have been argued to be sufficient to erase the signature of the dichotomy[7]; however, GEL depths do not represent the highly heterogeneous distribution of melt. The distribution varies with impact characteristics. For all but the highest energies (nominal crater size ≤10,000 km), melt is largely contained within the crustal excavation boundary and extends to depth (Figs 1 and 2). Depending on impact angle, 50–70% of the melt resides inside the excavation boundary, 25–30% is deposited outside the boundary and the remainder is ejected from the planet. Most re-deposited material is of crustal composition and results in a thickening of up to ~60% compared with the original crustal thickness.

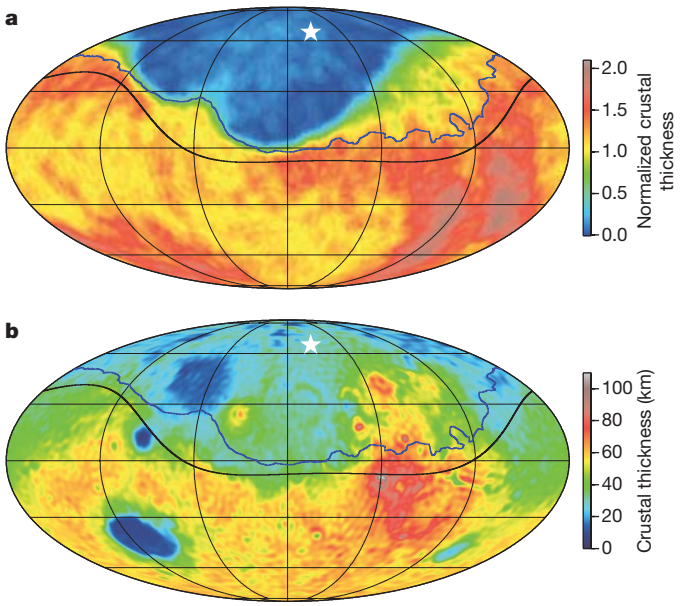

Figure 4 | A favoured impact hypothesis compared with Mars's crustal thickness. Post- to pre-impact simulation crustal thickness ratio (**a**), and model thicknesses (based on gravity and topography[10], revised by Neumann *et al.*, manuscript in preparation) (**b**). Superimposed are the Andrews-Hanna *et al.* dichotomy boundary[2] (black line) and the crustal excavation boundary from the simulation results (blue line). Impact simulation characteristics: 3.1×10^{29} J (nominal 10,000-km crater), 6 km s^{-1}, 45°, impactor diameter 2,230 km. Crustal excavation boundary centre[2] (star) shown at 66° N, 206° E. In **a**, the crustal thickness is computed at a 2° resolution and smoothed over a 10°-diameter cap area.

In areas where crust is removed and the mantle melts, fresh crust that crystallizes is likely to leave a difference in crustal thickness. The amount of mantle melt, and hence the thickness of the new crustal layer, is dependent on impact conditions.

For highly energetic and fast impacts, the shock wave produced is sufficiently strong to induce antipodal effects including crustal removal and melting. These are inconsistent with the lack of observed topographic, gravitational or magnetic anomalies antipodal to the proposed impact location. Thus we only consider viable simulations that produce antipodal features smaller than 10° in diameter.

We consider the effect of numerical resolution on the simulation results. The resolution and fidelity of post-impact crustal features in these simulations is higher than that of previous three-dimensional SPH studies. For simulations with a particle smoothing length of 150 km, the basin major axis, ellipticity, antipode size and melt cover differ from the nominal 118-km resolution simulations by an average of −8%, −1%, −28% and −16%, respectively, for nominal 10,000- and 12,000-km craters. Thus the qualitative conclusions are robust.

Combining the crust and melt distribution results, we find a 'sweet spot' in parameter space, where the simulations show striking similarity to the observed Mars dichotomy features (Figs 1, 3 and 4). Importantly, this range represents impact conditions that are probable in light of the age of the dichotomy[10] and probability distribution of the impact angle[11,22]. This parameter space 'sweet spot' is at impact energies of ~(3–6) × 10^{29} J, impact angles of 30–60° and impact velocities of 6–10 km s^{-1}, which imply impactor diameters of 1,600–2,700 km. These favoured simulation conditions encompass the range of uncertainty in the geometry of the observed crustal anomaly. The early age of the dichotomy is consistent with the expected timing of the influx of large impactors. These objects are also expected to have similar orbital velocities[23], resulting in impacts at or slightly above Mars's escape velocity (≥5 km s^{-1}). The most likely impact angle[11] is 45°.

Results from the large parameter space explored by the simulations provide new insights pertinent to global-scale impact processes thought to prevail in the early Solar System. Our simulations provide quantitative constraints for the previously only hypothesized extent of surface melting, planetary disruption and crustal removal as a function of impact energy and geometric characteristics. The predicted melt distribution over the surface may provide a heterogeneous geochemical signature observable by future Mars missions.

METHODS SUMMARY

SPH is a lagrangian method in which matter is represented by point masses smoothed over a particle radius (smoothing length), with density and internal energy computed according to kernel-weighted summation and by the conservation of mass, momentum and energy[16]. Pressure, as a function of internal energy and density, is computed with the Tillotson EOS, and pressure gradients and self-gravitating forces accelerate the particles. Our simulations conserve energy and angular momentum to better than 1 part in 2,000. Simulations are run for 26 h of model time, after which the r.m.s. particle velocity does not appreciably oscillate. We assume an olivine composition of $Fo_{75}Fa_{25}$ (ref. 24). Density ($\rho_0 = 3{,}500$ kg m^{-3}) (ref. 25), bulk modulus ($K = 131$ GPa) (ref. 26), heat capacity[26] and heat of vaporization ($H_{vap} = 10.013$ MJ kg^{-1}) (ref. 27) are measured material values; the nonlinear Tillotson compressive term (B) and two of the Tillotson EOS fitting parameters (b, U_0) are set to the average of those published for basalt, granite, anorthosite low- and high-pressure phases, and andesite ($B = 49$ GPa, $b = 1.4$, $U_0 = 550$ MJ kg^{-1}); b varies by only 8%. The remaining Tillotson EOS fitting parameters are identical for all given rocky materials ($a = 0.5$, $\alpha = 5$, $\beta = 5$). The olivine Hugoniot internal energy curve is on average 15% lower and 11% higher than the experimentally determined pure forsterite and fayalite curves, respectively, for 0–200 GPa. Using a forsterite EOS with Tillotson parameters fitted to the experimental curve results, on average, in 8% more melt (impacts of 8,000–12,000 km) and similar melt distribution. Both the mantle and crust are composed of olivine because a single-particle basalt layer would be numerically unresolved. The core is composed of iron and the impactor of basalt. The SPH code was modified to initialize with randomly distributed particles of prescribed composition, internal energy, pressure and mass as a function of radial position. Transient oscillations are damped

during a relaxation period run. The initial internal energy–pressure profile is set to that of hydrostatic equilibrium, whereas the surface and core-mantle boundary temperatures are set to those of parameterized convection models of Mars[28]. The internal energy–pressure–density profile is computed assuming adiabatic compression into the planet (core radius 1,600 km, central pressure 50 GPa, compatible with models[29,30]). The crustal excavation boundary size is a robust result: for a nominal 10,000-km crater, fitting the 20% and 80% crustal-fraction contours changes the boundary size by −9% and 12%, respectively.

Received 5 December 2007; accepted 23 April 2008.

1. Zuber, M. T. The crust and mantle of Mars. *Nature* **412,** 220–227 (2001).
2. Andrews-Hanna, J. C., Zuber, M. T. & Banerdt, W. B. The Borealis basin and the origin of the martian crustal dichotomy. *Nature* doi:10.1038/nature07011 (this issue).
3. Wilhelms, D. E. & Squyres, S. W. The martian hemispheric dichotomy may be due to a giant impact. *Nature* **309,** 138–140 (1984).
4. Zhong, S. J. & Zuber, M. T. Degree-1 mantle convection and the crustal dichotomy on Mars. *Earth Planet. Sci. Lett.* **189,** 75–84 (2001).
5. Frey, H. & Schultz, R. A. Large impact basins and the mega-impact origin for the crustal dichotomy on Mars. *Geophys. Res. Lett.* **15,** 229–232 (1988).
6. McGill, G. E. & Squyres, S. W. Origin of the martian crustal dichotomy – evaluating hypotheses. *Icarus* **93,** 386–393 (1991).
7. Hart, S. H., Nimmo, F., Korycansky, D. & Agnor, C. Probing the giant impact hypothesis of the martian crustal dichotomy. *Proc. 7th Int. Conf. Mars* abstr. 3332 (2007).
8. Nimmo, F. & Tanaka, K. Early crustal evolution of Mars. *Annu. Rev. Earth Planet. Sci.* **33,** 133–161 (2005).
9. Melosh, H. J. *Impact Cratering: A Geologic Process* (Oxford Univ. Press, New York, 1989).
10. Solomon, S. C. *et al.* New perspectives on ancient Mars. *Science* **307,** 1214–1220 (2005).
11. Shoemaker, E. M. in *Physics and Astronomy of the Moon* (ed. Kopal, Z.) 283–359 (Academic Press, New York, 1962).
12. Smith, D. E. *et al.* The global topography of Mars and implications for surface evolution. *Science* **284,** 1495–1503 (1999).
13. Aharonson, O., Zuber, M. T. & Rothman, D. H. Statistics of Mars' topography from the Mars Orbiter Laser Altimeter: slopes, correlations, and physical models. *J. Geophys. Res.* **106** (E10), 23723–23735 (2001).
14. Frey, H. V. *et al.* Ancient lowlands on Mars. *Geophys. Res. Lett.* **29,** doi:10.1029/2001GL013832 (2002).
15. Gault, D. E. & Wedekind, J. A. Experimental impact craters formed in water – gravity scaling realized. *Trans. Am. Geophys. Union* **59,** 1121 (1978).
16. Benz, W. in *Proc. NATO Adv. Res. Worksh. Numer. Modell. Nonlin. Stellar Puls.* (ed. Buchler, J. R.) 1–54 (Kluwer Academic, Boston, 1990).
17. Benz, W., Slattery, W. L. & Cameron, A. G. W. The origin of the Moon and the single-impact hypothesis. 1. *Icarus* **66,** 515–535 (1986).
18. Canup, R. M. & Asphaug, E. Origin of the Moon in a giant impact near the end of the Earth's formation. *Nature* **412,** 708–712 (2001).
19. Tillotson, J. H. *Metallic Equations of State for Hypervelocity Impact*. Report No. GA-3216, July 18 (General Atomic, San Diego, California, 1962).
20. Asimow, P. D. Magmatism and the evolution of the Earth's interior, in *Goldschmidt Conference Abstracts*, A40 ⟨http://www.goldschmidt2007.org⟩ (2007).
21. Cintala, M. J. & Grieve, R. A. Scaling impact melting and crater dimensions: implications for the lunar cratering record. *Meteorit. Planet. Sci.* **33,** 889–912 (1998).
22. Gilbert, G. K. The Moon's face, a study of the origin of its features. *Bull. Phil. Soc. Wash.* **12,** 241–292 (1893).
23. Canup, R. M. & Agnor, C. B. in *Origin of the Earth and Moon* (eds. Canup, R. M. & Righter, K.) 113–129 (Univ. Arizona Press, Tuscon, Arizona, 2000).
24. Sanloup, C., Jambon, A. & Gillet, P. A simple chondritic model of Mars. *Phys. Earth Planet. Inter.* **112,** 43–54 (1999).
25. Klein, C. *The Manual of Mineral Science* 22nd edn, 491–495 (Wiley, New York, 2002).
26. Anderson, D. L. & Isaak, D. G. in *Mineral Physics and Crystallography: A Handbook of Physical Constants* (ed. Ahrens, T. J.) 64–97 (American Geophysical Union, Washington DC, 1995).
27. Hashimoto, A. Evaporation metamorphism in the early solar nebula – evaporation experiments on the melt FeO-MgO-SiO_2-CaO-Al_2O_3 and chemical fractionations of primitive materials. *Geochem. J.* **17,** 111–145 (1983).
28. Hauck, S. A. & Phillips, R. J. Thermal and crustal evolution of Mars. *J. Geophys. Res.* **107** (E7), doi:10.1029/2001JE001801 (2002).
29. Yoder, C. F. *et al.* Fluid core size of Mars from detection of the solar tide. *Science* **300,** 299–303 (2003).
30. Bertka, C. M. & Fei, Y. W. Density profile of an SNC model martian interior and the moment-of-inertia factor of Mars. *Earth Planet. Sci. Lett.* **157,** 79–88 (1998).

Supplementary Information is linked to the online version of the paper at www.nature.com/nature.

Acknowledgements We thank F. Nimmo, M. Zuber, J. Andrews-Hanna and R. Canup for discussions, J. Melosh for comments, and S. Squyres for suggesting the problem and the approach more than a decade ago. This work was supported by the Henshaw Fellowship, the Natural Sciences and Engineering Research Council of Canada and the Canadian Space Agency.

Author Information Reprints and permissions information is available at www.nature.com/reprints. Correspondence and requests for materials should be addressed to M.M.M. (mmm@caltech.edu).